

## ■ Drug Delivery

# Alternating Magnetic Field Controlled Targeted Drug Delivery Based on Graphene Oxide-Grafted Nanosupramolecules

Bing Zhang,<sup>[a, b]</sup> Qilin Yu,<sup>[c]</sup> and Yu Liu\*<sup>[a, b]</sup>

**Abstract:** Graphene oxide (GO)-grafted nanosupramolecules have recently emerged as neoteric nano drug carriers in the therapy of refractory diseases. Herein, a multicomponent nanosupramolecular drug carrier based on a targeted peptide and magnetic GO is reported, the drug-release behavior of which can be regulated by an alternating magnetic field (AMF). This multicomponent nanosupramolecular carrier is composed of  $\beta$ -cyclodextrin ( $\beta$ -CD)/nickel nanoparticle-modified graphene oxide (GONiCD) and mitochondrial ion-targeting peptide (MitP)-grafted hyaluronic acid (HAMitP). Owing to the host-guest interaction between  $\beta$ -cyclodextrin and the cyclohexyl groups on MitP, GONiCD and HAMitP could

form supramolecular assemblies during the doxorubicin (Dox) loading process, which not only remarkably enhances the drug-loading capacity, but also improves the drug-release efficiency under AMF stimulus. During co-incubation with tumor cells, the Dox-loaded assemblies could strongly target the tumor mitochondria and damage both the mitochondria and the nuclei, owing to Dox release from the assemblies induced by AMF. This study sheds light on the exploration of peptide caps for controlled drug loading/release of supramolecular nanocarriers for efficient drug delivery and anticancer therapy.

## Introduction

With the rapid development of nanotechnology, abundant nanocarriers, for example, mesoporous silica nanoparticles, liposomes, and polymeric nanoparticles (NPs), have been designed for drug delivery in cancer therapy.<sup>[1]</sup> Supramolecular nanocarriers are an emerging kind of nanocarriers that are constructed by host-guest or other interactions.<sup>[2]</sup> Compared with traditional nanocarriers, supramolecular nanocarriers are multi-stimuli responsive, highly efficient for drug release, and easy to load with drugs, owing to the dynamic interaction between the building blocks and drugs.<sup>[3]</sup> A series of host molecules, such as cyclodextrins (CDs), pillararenes, and cucurbituril, have been used in construction of supramolecular nanocarriers for stimuli-responsive drug delivery.<sup>[4]</sup>

On the other hand, graphene oxides (GOs), as the main two-dimensional nano-assembly matrix, which have the advantages

of large surface area, good biocompatibility, and high feasibility of loading a wide range of drugs, have shown promising application prospects and attracted more and more attention.<sup>[5]</sup> Recently, the combination of GO with supramolecules or other further modifications also exhibited excellent performance in drug delivery.<sup>[6]</sup> In combination with supramolecular host-guest components, GOs have been developed as building blocks to construct supramolecular assemblies for targeted drug delivery, photothermal killing of tumor cells, and inhibition of tumor metastasis.<sup>[7]</sup> However, in drug-delivery applications, the drug-loading and stimulus-responsive drug-releasing efficiency of GO-based two-dimensional nanocarriers remain to be improved. To the best of our knowledge, there is no report on designing smart stimuli-responsive GO assemblies for enhancement of their drug-loading and drug-releasing capacity.

One focus of nanocarrier construction is design of multi-stimuli-responsive caps for controlled release of drugs.<sup>[8]</sup> Numerous supramolecular caps, which are based on the interaction between macrocyclic hosts (cyclodextrin, cucurbituril, etc.) and their corresponding guest molecules, have been developed to respond to different environmental stimuli, for example, heat, light, pH, oxidizing/reducing agents, enzymes, and alternating magnetic field (AMF).<sup>[9]</sup> All of them, except AMF-responsive systems, exhibited lots of shortages, such as limited penetration and poor adjustment. In contrast, AMF-responsive supramolecular caps exhibit outstanding advantages, owing to the properties of noninvasiveness, deep penetration, and easy control of the AMF stimulus.<sup>[10]</sup> In AMF-responsive capping systems, magnetic nanocomposites (e.g., Fe-, Co-, Mn-, or Ni-derived materials) may produce heat energy under AMF stimulus, leading to the departure of heat-responsive caps from the

[a] Dr. B. Zhang, Prof. Y. Liu  
College of Chemistry  
State Key Laboratory of Elemento-Organic Chemistry  
Nankai University, Tianjin 300071 (P.R. China)  
E-mail: yuliu@nankai.edu.cn

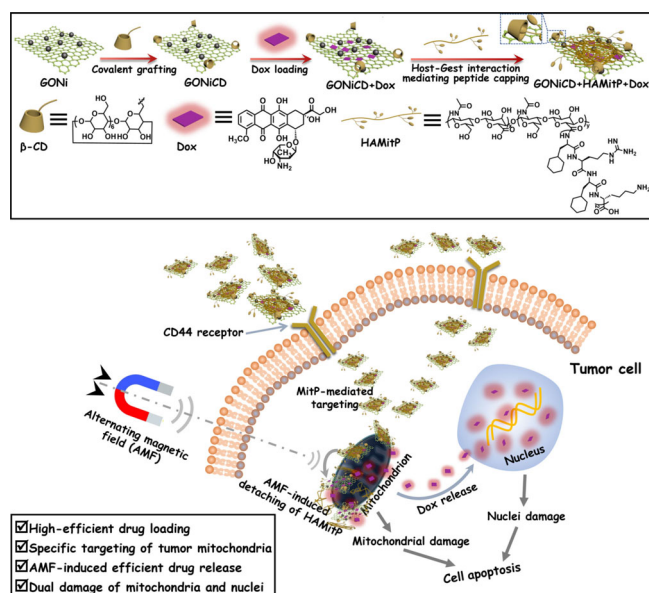
[b] Dr. B. Zhang, Prof. Y. Liu  
Collaborative Innovation Center of Chemical Science and Engineering  
Tianjin 300072 (P. R. China)

[c] Q. Yu  
Key Laboratory of Molecular Microbiology and Technology  
Ministry of Education, College of Life Sciences  
Nankai University, Tianjin 300071 (P.R. China)

 Supporting information and the ORCID identification number(s) for the author(s) of this article can be found under:  
<https://doi.org/10.1002/chem.202003328>

nanocomposites and consequent drug release. Although several AMF-responsive caps, for example, *N*-(6-aminoethyl)amino-methyltriethoxysilane stalk-binding cucurbit[6]uril (CB[6]), 4,4'-azobis(4-cyanovaleic acid)-linked CD, and poly(*N*-isopropylacrylamide), have been designed,<sup>[11]</sup> other kinds of AMF-sensitive caps, especially those capping two-dimensional nanocarriers, remain to be developed.

In this study, we developed a peptide-capped GO supramolecular assembly for drastic enhancement of drug-loading and drug-releasing capacity to realize efficient drug delivery. With supramolecular-interaction-mediated peptide capping and drug loading of the GO supramolecular assembly, this multicomponent carrier realized both high-efficiency drug loading and AMF-sensitive drug release. The nanoplatform was constructed from  $\beta$ -CD-grafted and Ni nanoparticle (NiNP)-decorated GO (GONiCD), together with mitochondrion-targeting peptide (MitP)-grafted hyaluronic acid (HA) specifically binding to tumor cell CD44 receptor (HAMitP; Scheme 1). Owing to the capping activity of MitP on the HA polymer, the GONiCD + HAMitP assemblies not only have improved colloidal stability and drug-loading capacity because of the constraining effect of HA, but also exhibit higher drug-releasing efficiency compared with GONiCD alone. Moreover, the doxorubicin (Dox)-loaded assemblies strongly targeted to the mitochondria of tumor cells, followed by severe damage to both the mitochondria and the nuclei for inducing tumor cell apoptosis through AMF-triggered efficient release of Dox. This study supplies a novel drug-delivery approach that is much better than that of the traditional multicomponent assemblies, and sheds light on the exploration of promising peptide caps for controlled drug release from two dimensional nanoplatforms for cancer therapy.



**Scheme 1.** Illustration of construction of the AMF-driven supramolecular nanocarriers for inducing tumor cell apoptosis.

## Results and Discussion

GO was synthesized by a modified Hummer's method (Figure 1a).<sup>[12]</sup> Owing to the presence of metal-ion-chelating carboxyl and carbonyl groups,  $\text{Ni}^{2+}$  was easily adsorbed into GO and then reduced to NiNPs on the surface by  $\text{NaBH}_4$ , generating GONi (Figure 1a). Mono-6-deoxy-6-ethylenediamino- $\beta$ -CD was further grafted to GONi by the EDC/NHS reaction, to obtain the final GONiCD nanosheets (Figure 1a). TEM revealed that GO, GONi, and GONiCD had membrane/sheetlike morphology with lateral sizes of 300–500 nm. Compared with GO, both GONi and GONiCD had randomly distributed NiNPs with sizes of 5–10 nm on the surface of GO nanosheets (Figure 1a, Figure S1 in the Supporting Information). FTIR spectroscopy indicated that GO, GONi, and GONiCD have an adsorption peak at 1770–1740  $\text{cm}^{-1}$ , indicating COOH in these nanosheets. The presence of COOH in GONi suggested that COOH groups were only partially reduced by hydrazine monohydrate during production of NiNPs. Moreover, the final GONiCD nanosheets had the adsorption peaks at 2850  $\text{cm}^{-1}$  (C–H) and 3440–3300  $\text{cm}^{-1}$  (CONH) (Figure 1b), indicating successful grafting of  $\beta$ -CD on GONi by amide bonds. A SQUID assay at 300 K showed that GONiCD had a saturation magnetization of 57  $\text{emu g}^{-1}$  with no obvious hysteresis loop (Figure S2 in the Supporting Information), and thus validated the superparamagnetic property of GONiCD. In an AMF (375 kHz, 5 kW), the GONiCD solution showed a rapid increase of the temperature, which reached 54 °C after 10 min (Figure S3 in the Supporting Information). The specific loss power of GONiCD was calculated to be 906.5 and 700  $\text{W g}^{-1}$ , respectively, indicating excellent heating efficiency of GONiCD for AMF-triggered drug release, which was attributed to the good magnetism-responsive property of NiNPs.

To synthesize the peptide-modified tumor-targeting polymer HAMitP, the mitochondrion-targeting peptide MitP was covalently linked to HA by the EDC/NHS reaction (Figure S4 in the Supporting Information). FTIR spectra revealed the presence of  $\text{CH}_2$  and CONH in HAMitP, indicating successful grafting of

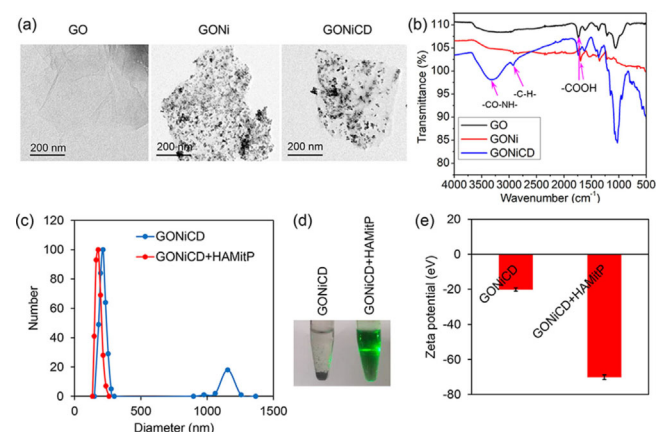


**Figure 1.** Characterization of GO, GONi, GONiCD, and the GONiCD + HAMitP supramolecular nanocarriers. a) TEM images of GO, GONi, and GONiCD. b) FTIR spectra. c) Size distribution of GONiCD and GONiCD + HAMitP. d) Tyndall effect. e) Zeta potential.

MitP onto the HA polymer (Figure S5 in the Supporting Information).

Since cyclohexylalanine of MitP could bind  $\beta$ -CD by host-guest interaction, in which the cyclohexyl group and  $\beta$ -CD have an association constant  $K_a$  of approximately 800, GONiCD and HAMitP can form supramolecular assemblies by multivalent binding.<sup>[13]</sup> To confirm the formation of this assembly, dynamic light scattering and zeta-potential analysis of both GONiCD and GONiCD + HAMitP were performed. GONiCD had two size distribution peaks at 200 and 1200 nm, indicating some aggregation of GONiCD. In contrast, GONiCD + HAMitP had only one size distribution peak at approximately 200 nm (Figure 1c). Consistently, whereas GONiCD slowly precipitated from the solution to the bottom of the tubes, the solution of GONiCD + HAMitP remained stable and had an obvious Tyndall effect under irradiation with a visible-light laser (Figure 1d). Moreover, GONiCD + HAMitP had a more negative zeta potential than GONiCD ( $-70$  versus  $-19$  mV, Figure 1e), which was attributed to the binding of negatively charged HAMitP to GONiCD. These results confirmed that GONiCD and HAMitP could effectively interact with each other to form supramolecular assemblies, which increase the colloidal stability of the 2D nanosheets in aqueous solution.

Since GO can adsorb abundant chemotherapeutic drugs (e.g., Dox, paclitaxel, camptothecin) owing to  $\pi$ - $\pi$  stacking and electrostatic attraction, the GO platform has a potential as a drug-delivery carrier of these drugs.<sup>[14]</sup> The drug loading capacity of GONiCD and the GONiCD + HAMitP supramolecular assemblies was investigated with the model chemotherapeutic drug Dox. After 24 h of incubation between GONiCD or GONiCD + HAMitP and Dox, the nanocomposites were centrifuged and the decreased concentrations of the supernatants were measured as the loaded Dox contents. Whereas GONiCD only exhibited a loading capacity of approximately 18 wt%, GONiCD + HAMitP showed a loading capacity of  $>36$  wt% (Figure 2a), which indicated that formation of the supramolecular assemblies enhanced the Dox loading of the 2D nanosheets. The loading capacity of the assemblies is even higher than those of the commonly used drug-delivery systems, for example, mesoporous silica nanoparticles with a loading capacity of  $<25$ %.<sup>[15]</sup>

To investigate the mechanism by which the supramolecular assembly enhanced drug-loading capacity, fluorescence polarization (FP) assays were performed to indicate the interaction strength between Dox and the nanocomposites, in which high FP values indicate strong interaction. Dox-loaded GONiCD or GONiCD + HAMitP was treated by heating at  $55^\circ\text{C}$  for 10 min, followed by slow cooling to  $15^\circ\text{C}$  over 20 min, and the FP values of the samples were measured in real time. The FP values of Dox-loaded GONiCD + Dox suddenly decreased to approximately 20 during the heating period, and then gradually increased to  $>60$  (Figure 2b), that is, the interaction between GONiCD and Dox was severely impaired by heating and recovered by low temperature ( $15^\circ\text{C}$ ). In contrast, the FP value of GONiCD + HAMitP + Dox was reduced to 42 by heating, and then increased to approximately 60 during cooling (Figure 2b). Moreover, the addition of L-cyclohexyl alanine (CA), a competi-

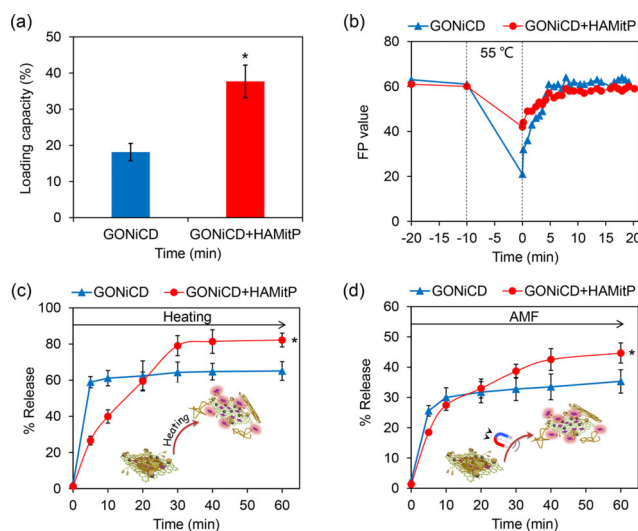


**Figure 2.** Dox-loading and -release capacity of GONiCD and GONiCD + HAMitP. a) Dox loading capacity. b) Heating-induced change of the FP of Dox-loaded GONiCD and GONiCD + HAMitP. The Dox-loaded nanocomposites were treated by heating at  $55^\circ\text{C}$  from  $-10$  to  $0$  min, followed by slow cooling to  $15^\circ\text{C}$  at a rate of  $2^\circ\text{C min}^{-1}$  (from  $0$  to  $20$  min). c) Release of Dox induced by heating at  $55^\circ\text{C}$ . d) Release of Dox induced by AMF ( $375$  kHz,  $5$  kW).

tive molecule of cyclohexyl in MitP to  $\beta$ -CD for disruption of supramolecular assembly, severely decreases the Dox-loading capacity of the mixture of GONiCD + HAMitP (Figure S6 in the Supporting Information). These results suggest that the enhancement of Dox-loading capacity by supramolecular assembly can be attributed to increased interaction strength between GONiCD + HAMitP and the drug even at a high temperature.

Since the interaction strength between Dox and the assemblies could be affected by heating, bulk heating, or magnetic heating by AMF, which in turn may trigger release of Dox, we next attempted to take advantage of this to regulate the release of Dox. Under no stimulus of bulk heating or AMF, both GONiCD and GONiCD + HAMitP only release quite low levels of Dox ( $<5$ %) even after 60 min of incubation (Figure S7 in the Supporting Information). Remarkably, heating by a metal bath triggered rapid release of Dox from both GONiCD and GONiCD + HAMitP. This direct heating triggered more Dox release from the GONiCD + HAMitP than from GONiCD ( $\approx 80$ % versus  $\approx 60$ %) after 30 min (Figure 2c). Interestingly, GONiCD + HAMitP reached its stable degree of Dox release after 30 min, whereas GONiCD reached it in only 5 min (Figure 2c), that is, the interaction between the drug and the assemblies is stronger than that between the drug and GONiCD. Similar results were observed when the drug-loaded nanocomposites were treated with an AMF. Under AMF treatment, GONiCD + HAMitP exhibited higher Dox-release capacity than GONiCD ( $46$ % versus  $35$ %, Figure 2d). Together, these results revealed that the GONiCD + HAMitP assemblies had higher Dox-loading and Dox-releasing capacity than GONiCD.

To evaluate the drug-release and nucleus-damage ability of the GONiCD + HAMitP + Dox nanocarrier in tumor cells, we in-

cubated the drug-loaded nanocarriers with PANC-1 tumor cells and monitored the fluorescence distribution of Dox by confocal microscopy. Fluorescence quantification of intracellular Dox revealed that the cells incubated with GONiCD + HAMitP + Dox had a slight higher Dox uptake than with GONiCD + Dox or Dox alone (1.3-fold vs. GONiCD + Dox and 1.6-fold vs. Dox; Figure S8 in the Supporting Information), indicating that HAMitP in combination with GONiCD facilitated uptake of Dox by the tumor cells. We also added fluorescein isothiocyanate-tagged 1-adamantanemethylamine (FITC-Ada) to indicate distribution of GONiCD owing to the strong supramolecular interaction between Ada and  $\beta$ -CD. After 12 h of co-incubation, both Dox-loaded GONiCD and GONiCD + HAMitP exhibited intracellular distribution, as indicated by the green fluorescence of FITC-Ada (Figure 3 a and c). For GONiCD, Dox was mainly co-localized with FITC-Ada, that is, Dox remained in the nanosheets. Moreover, AMF treatment caused a slight decrease of the Pearson's correlation coefficient (PCC) from 0.94 to 0.75, suggesting some release of Dox from GONiCD (Figure 3 b). Co-localization of Dox and the nucleus dye Hoechst 33342 further revealed an obvious increase in PCC between them on AMF treatment (Figure 3 b). Therefore, AMF led to Dox release from GONiCD to the cytoplasm and to the nucleus to some extent.

Notably, for the GONiCD + HAMitP + Dox group, as opposed to the GONiCD + Dox group (Figure 3 a, bottom), AMF treatment caused most of the Dox to not co-localize with FITC-Ada and distribute throughout the cells (Figure 3 c, bottom), and the PCC between Dox and FITC-Ada decreased from 0.82 to 0.24 (Figure 3 d). These observations indicated that GONiCD + HAMitP had much higher Dox release efficiency than GONiCD in the cells under AMF stimulus, although they had not so distinct release efficiency as compared with GONiCD under cell-free conditions (Figure 2 c and d). This could be explained by the interaction between HAMitP and the intracellular organelles (e.g., the mitochondria) reducing the interaction strength

between HAMitP and Dox and thus facilitating Dox release from the assemblies. Moreover, the PCC between Dox and Hoechst 33342 clearly increased from  $-0.08$  to  $0.5$  (Figure 3 d). The preferential distribution of Dox in the nuclei might be attributed to AMF-triggered Dox release from the assemblies and further Dox targeting to the nuclei. Remarkably, GONiCD + HAMitP + Dox caused severe nucleus fragmentation (indicated by yellow arrows in Figure 3 c) under AMF treatment, whereas GONiCD alone did not cause this fragmentation (Figure 3 a). Together, these results indicated that AMF treatment distinctly promoted Dox release from the assemblies, enhanced nucleus entry of Dox, and consequently induced severe nucleus damage.

Since MitP is designed as a typical targeting molecule for mitochondria binding, we speculated that the presence of HAMitP on the host might lead to targeting of the assemblies to mitochondria and impair the function of this organelle owing to the drug-loaded 2D nanocarriers. Confocal microscopy indicated that FITC-labeled GONiCD + HAMitP was localized mainly at the mitochondria in PANC-1 tumor cells, whereas GONiCD alone scarcely co-localized with the mitochondria (Figure 4 a). Consistently, the PCC value between FITC-Ada and Mitotracker Red for the GONiCD + HAMitP assemblies was much higher than for GONiCD alone ( $0.63$  versus  $0.18$ , Figure 4 b), and this confirms the high mitochondrion-targeting activity of the assemblies.

We then investigated whether the drug-loaded assemblies might disrupt the mitochondria of tumor cells. Western blotting revealed that treatment with GONiCD + HAMitP + Dox assemblies caused higher levels of cytochrome c release from the mitochondria to the cytoplasm than did treatment with other contrast materials or Dox alone (Figure 4 c), that is, both

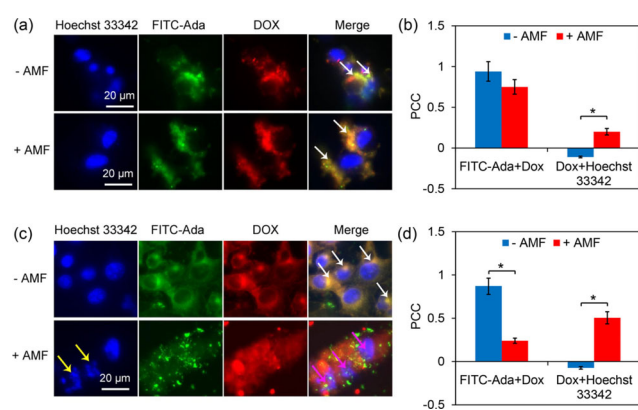


**Figure 3.** Dox release and nucleus damage in PANC-1 tumor cells caused by the 2D supramolecular nanocarriers. a) Confocal images of the cells treated with GONiCD + Dox. The white arrows indicate co-localization between FITC-tagged nanocarriers and Dox. b) PCC analysis of the confocal images in a). c) Confocal images of the cells treated with GONiCD + HAMitP + Dox. The yellow arrows indicate fragmented nuclei. The purple arrows indicate co-localization between Dox and nuclei. d) PCC analysis of the confocal images in c). Asterisks indicate significant differences between the groups ( $P < 0.05$ ).

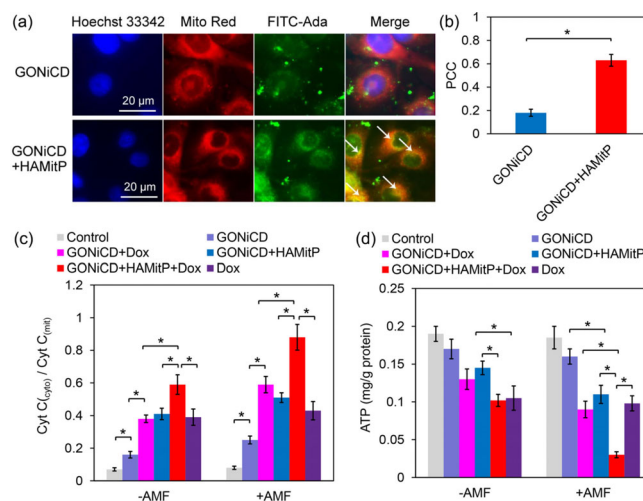


**Figure 4.** Mitochondrion targeting and damage by the 2D supramolecular nanocarriers in PANC-1 tumor cells. a) Confocal images of the tumor cells treated with GONiCD or GONiCD + HAMitP, followed by Mitotracker Red (Mito Red) and Hoechst 33342 staining. The white arrows indicate co-localization between the nanocarriers and mitochondria. b) PCC analysis of the confocal images in a). c) Ratio of cytosolic cytochrome c ( $Cyt C_{(cyto)}$ ) to mitochondrial cytochrome c ( $Cyt C_{(mit)}$ ) in the tumor cells treated with the nanocomposites or Dox alone. d) Intracellular ATP levels. Asterisks indicate significant differences between the groups ( $P < 0.05$ ).

Dox and the assemblies contributed to severe mitochondrial damage. More importantly, AMF aggravated mitochondrial damage of the tumor cells treated with GONiCD+HAMitP+Dox assemblies, with the ratio of cytochrome c in the cytoplasm to that in the mitochondria increasing from 0.59 to 0.88 (Figure 4c). Consistent with this, ATP assay further revealed that intracellular ATP levels were decreased by the assemblies, and this decrease was deteriorated by AMF treatment (Figure 4d). Therefore, the drug-loaded assemblies had the strongest activity in damaging the mitochondria and impairing energy production in the tumor cells.

The antitumor effect of the 2D supramolecular nanocarriers on PANC-1 tumor cells on exposure to AMF was evaluated by an Annexin V/PI staining experiment. Confocal microscopy indicated that GONiCD+Dox, GONiCD+HAMitP, Dox, and GONiCD+HAMitP+Dox can induce tumor cell apoptosis and necrosis with the aid of AMF (Figure 5a). Among these four treatments, GONiCD+HAMitP+Dox induced the highest degrees of apoptosis (78.3%) and necrosis (18.2%), as shown in Figure 5b and c, respectively. The highest antitumor activity of GONiCD+HAMitP+Dox was confirmed by CCK-8 assays, which showed that cell viability decreased to 18% with the aid of AMF (Figure S9 in the Supporting Information). However, for the normal 293T cells, while Dox alone at a concentration comparable to that in the assemblies exhibited obvious toxicity, GONiCD+HAMitP+Dox had no obvious impact on cell viability (Figure S10 in the Supporting Information), which may be attributed to poor targeting capacity of the assemblies to normal cells. In addition, even with the same contents of loaded Dox (18.1%), the GONiCD+HAMitP assemblies exhibited higher release capacity and higher impact on tumor cell viability (Figure S11 in the Supporting Information), and this indicates that the higher release capacity of the GONiCD+HAMitP assemblies is involved in their higher anticancer ability. These results suggested that the 2D supramolecular nanocarriers

could effectively carry the anticancer drug Dox into the cells, release the drug with the aid of AMF, and consequently induce nucleus damage and kill most of the tumor cells, while the toxicity of the anticancer drug to normal cells is diminished.

## Conclusion

This study developed a new approach for construction of multicomponent nanosupramolecular assemblies with AMF-stimulus responsivity for high-efficiency carrying of antitumor drugs. The 2D nanocarriers are composed of  $\beta$ -CD/NiNP-decorated GOs (GONiCD) and MitP-modified HA (HAMitP). Owing to the capping function of the MitP peptide, the GONiCD+HAMitP assemblies not only exhibit the drug-loading capacity of the 2D nanosheets, but also efficiently release Dox under exposure to AMF. After co-incubation of the drug-loading assemblies with tumor cells, the assemblies could target the mitochondria, efficiently release Dox to both the mitochondria and nuclei, and finally cause cell death. This study sheds light on the development of promising AMF-regulated peptide caps for two-dimensional nanocarriers, and encourages us to design feasible and convenient polymer-based supramolecular assemblies for efficient anticancer therapy. Further investigations will focus on exploring the application of the nanoplatforms to co-deliver anticancer drugs and other auxiliary agents (e.g., RNA, immune agonists) for in vivo applications.

## Acknowledgements

We thank for the financial supporting of National Natural Science Foundation of China (nos. 21772099, 31870139, 21861132001) and China Postdoctoral Science Foundation (no. 2018M641632).

## Conflict of interest

The authors declare no conflict of interest.

**Keywords:** drug delivery • graphene • magnetic properties • nanostructures • supramolecular chemistry

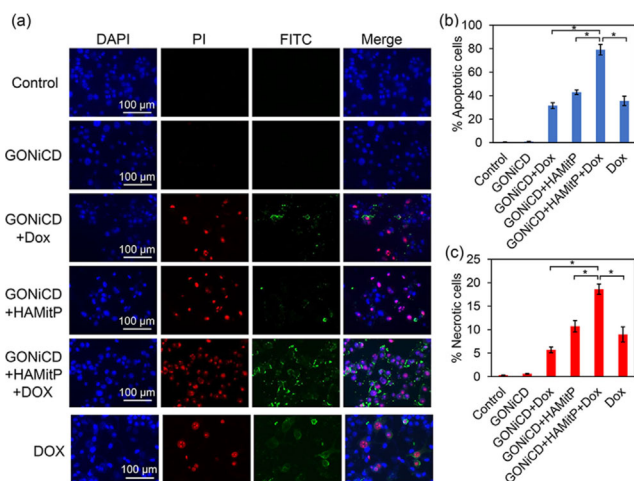


**Figure 5.** Apoptosis induced by the 2D supramolecular nanocarriers in PANC-1 tumor cells with the aid of AMF. a) Confocal images of the tumor cells treated with GONiCD, GONiCD+Dox, GONiCD+HAMitP, GONiCD+HAMitP+Dox, or Dox, followed by FITC-Annexin V/PI and Hoechst 33342 staining. b) Statistical analysis of apoptotic cells. c) Statistical analysis of necrotic cells. Asterisks indicate significant differences between the groups ( $P < 0.05$ ).

- [5] a) Z. Li, N. Song, Y. W. Yang, *Matter* **2019**, *1*, 345–368; b) R. Garriga, I. Jurawicz, E. Romero, C. Jarne, V. L. Cebolla, A. B. Dalton, E. Muñoz, *ACS Appl. Mater. Interfaces* **2016**, *8*, 1913–1921.
- [6] a) Y. Wang, M. Qiu, M. Won, E. Jung, T. Fan, N. Xie, J. S. Kim, *Coord. Chem. Rev.* **2019**, *400*, 213041; b) S. M. Mousavi, S. A. Hashemi, Y. Ghaseemi, A. M. Amani, A. Babapoor, O. Arjmand, *Drug Metabolism Rev.* **2019**, *51*, 12–41; c) C. Chung, Y. K. Kim, D. Shin, S. R. Ryoo, B. H. Hong, D. H. Min, *Acc. Chem. Res.* **2013**, *46*, 2211–2224.
- [7] a) B. Zhang, Q. Yu, Y. M. Zhang, Y. Liu, *Chem. Commun.* **2019**, *55*, 12200–12203; b) Y. M. Zhang, Y. Cao, Y. Yang, J. T. Chen, Y. Liu, *Chem. Commun.* **2014**, *50*, 13066–13069; c) J. Liu, K. Liu, L. Feng, Z. Liu, L. Xu, *Biomater. Sci.* **2017**, *5*, 331–340.
- [8] a) R. R. Castillo, D. Lozano, B. González, M. Manzano, I. Izquierdo-Barba, M. Vallet-Regí, *Expert Opinion Drug Delivery* **2019**, *16*, 415–439; b) M. Moros, J. Idiago-López, L. Asín, E. Moreno-Antolín, L. Beola, V. Grazú, J. M. de la Fuente, *Adv. Drug Delivery Rev.* **2019**, *138*, 326–343; c) J. Wankar, N. G. Kotla, S. Gera, S. Rasala, A. Pandit, Y. A. Rochev, *Adv. Funct. Mater.* **2020**, *30*, 1909049.
- [9] a) J. Lu, E. Choi, F. Tamanoi, J. I. Zink, *Small* **2008**, *4*, 421–426; b) M. Koo, K. T. Oh, G. Noh, E. S. Lee, *ACS Appl. Mater. Interfaces* **2018**, *10*, 24450–24458; c) Y. J. Ho, C. H. Wu, Q. F. Jin, C. Y. Lin, P. H. Chiang, N. Wu, C.-H. Fan, C.-M. Yang, C. K. Yeh, *Biomaterials* **2020**, *232*, 119723; d) D. Mertz, O. Sandre, S. Begin-Colin, *Biochim. Biophys. Acta Gen. Subj.* **2017**, *1861*, 1617–1641; e) N. Singh, A. Karambelkar, L. Gu, K. Lin, J. S. Miller, C. S. Chen, M. J. Sailor, S. N. Bhatia, *J. Am. Chem. Soc.* **2011**, *133*, 19582–19585; f) P. T. Wong, S. K. Choi, *Chem. Rev.* **2015**, *115*, 3388–3432.
- [10] a) J. H. Lee, K. J. Chen, S. H. Noh, M. A. García, H. Wang, W. Y. Lin, H. R. Tseng, *Angew. Chem. Int. Ed.* **2013**, *52*, 4384–4388; *Angew. Chem.* **2013**, *125*, 4480–4484; b) C. S. Kumar, F. Mohammad, *Adv. Drug Delivery Rev.* **2011**, *63*, 789–808.
- [11] a) C. R. Thomas, D. P. Ferris, J. H. Lee, E. Choi, M. H. Cho, E. S. Kim, J. F. Stoddart, J.-S. Shin, J. Cheon, J. I. Zink, *J. Am. Chem. Soc.* **2010**, *132*, 10623–10625; b) W. Chen, C. A. Cheng, J. I. Zink, *ACS Nano* **2019**, *13*, 1292–1308; c) Z. Tian, X. Yu, Z. Ruan, M. Zhu, Y. Zhu, N. Hanagata, *Microporous and Mesoporous Mater.* **2018**, *256*, 1–9.
- [12] J. Chen, B. Yao, C. Li, G. Shi, *Carbon* **2013**, *64*, 225–229.
- [13] a) Q. Yu, Y. M. Zhang, Y. H. Liu, X. Xu, Y. Liu, *Sci. Adv.* **2018**, *4*, eaat2297; b) Q. Yu, Y. M. Zhang, Y. H. Liu, Y. Liu, *Adv. Therapeutics* **2019**, *2*, 1800137.
- [14] a) S. F. Kiew, L. V. Kiew, H. B. Lee, T. Imae, L. Y. Chung, *J. Controlled Release* **2016**, *226*, 217–228; b) L. Zhang, J. Xia, Q. Zhao, L. Liu, Z. Zhang, *Small* **2010**, *6*, 537–544; c) F. Nasrollahi, J. Varshosaz, A. A. Khodadadi, S. Lim, A. Jahanian-Najafabadi, *ACS Appl. Mater. Interfaces* **2016**, *8*, 13282–13293.
- [15] a) P. Eskandari, B. Bigdeli, M. Porgham Daryasari, H. Baharifar, B. Bazri, M. Shourian, A. A. Saboury, *J. Drug Targeting* **2019**, *27*, 1084–1093; b) G. Yang, H. Gong, X. Qian, P. Tan, Z. Li, T. Liu, Z. Liu, *Nano Res.* **2015**, *8*, 751–764; c) H. Meng, M. Liong, T. Xia, Z. Li, Z. Ji, J. I. Zink, *ACS Nano* **2010**, *4*, 4539.

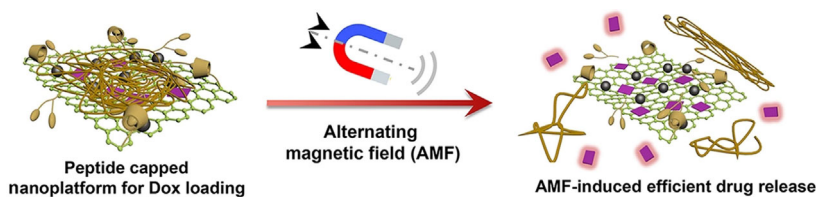
---

Manuscript received: July 15, 2020

Accepted manuscript online: July 21, 2020

Version of record online: ■■■■■ 0000

## FULL PAPER



**Supramolecular nanocarriers deliver:** Multicomponent graphene oxide-grafted cyclodextrin-based nanosupramolecular assemblies were developed for high-efficiency delivery of antitumor drugs. Owing to the responsiveness of the capping peptide to alternating mag-

netic field (AMF), the assemblies exhibit efficient AMF-induced drug release. After co-incubation with tumor cells, drug-loaded assemblies could target the mitochondria, efficiently release the drug to both the mitochondria and nuclei, and finally cause cell death.

## Drug Delivery

B. Zhang, Q. Yu, Y. Liu\*



Alternating Magnetic Field Controlled Targeted Drug Delivery Based on Graphene Oxide-Grafted Nanosupramolecules 